PECVD, RF vs Dual Frequency: investigation of plasma influence on metalorganic precursors decomposition and material characteristics

Fabien Piallat, Christophe Vallée, Rémy Gassilloud, Philippe Michallon, Bernard Pélissier, Pierre Caubet

PECVD RF versus dual frequency: an investigation of plasma influence on metal–organic precursors' decomposition and material characteristics

F Piallat[1,2,3], C Vallée[3,4], R Gassilloud[2], P Michallon[2], B Pelissier[3] and P Caubet[1]

[1] STMicroelectronics, 850 rue Jean Monnet, 38920 Crolles, France
[2] CEA, LETI, CAMPUS Minatec, 17 rue des Martyrs, F-38054 Grenoble Cedex 9, France
[3] LTM-CNRS, 17 rue des Martyrs, 38054 Grenoble, France

Abstract

Plasma enhanced metal organic chemical vapor deposition (PEMOVCD) of titanium nitride with dual frequency plasma sources were studied by means of plasma and material characterization. Adding a low frequency to a radio frequency plasma in order to enhance the deposition reaction mechanism is demonstrated. An in depth investigation of plasma by optical emission spectroscopy shows that due to secondary electrons heating the plasma, it enters a gamma-mode and that LF permits better dissociation of the H_2 reactant gas. Moreover, it appears that the TiN metal organic precursor is not completely dissociated (no Ti^* emission) but new species are observed that indicate a different fragmentation of the precursor. When LF plasma is used these modifications can be correlated to a change in the deposition reaction mechanism which affects the properties of the deposited material. Strong modifications of the TiN properties and deposition rate are observed when adding 17–60 W LF to a 200 W RF plasma. For example, with 35 W LF added to a 200 W RF, the deposition rate is increased by a factor two and the film appears to be less resistive (by 50%) and has a higher density. Such effects are not observed when only increasing the RF power (from 200 to 300 W with no LF power).

Keywords: dual-frequency plasma, MOCVD, metal, XPS, OES

1. Introduction

In a plasma enhanced metal–organic chemical vapour deposition (PEMOCVD), dissociation of the precursor affects the chemical, physical and electrical properties of the deposited film as well as the growth rate and conformity of the process. In a capacitively coupled plasma (CCP) reactor with a fixed radio frequency (RF), the electron density is known to increase with the plasma power and the electron temperature is known to vary with the pressure. Thus, if one wants to modify the dissociation rate of a given precursor, pressure and power have to be carefully tuned. Another parameter often not taken into account, but that should be considered, is the plasma frequency. Flamm, in 1986, studied the plasma frequency effect in low-pressure plasma etching [1]. He showed that frequency alters many plasma parameters such as the spatial distribution of species, their energies and concentrations as a function of time, and energies of ions impinging the substrate. In their simulation paper, Surendra and Graves predicted that higher RF frequencies would produce higher plasma densities for the same voltage [2]. Also, faster plasma etching can be obtained

[4] Author to whom any correspondence should be addressed.
E-mail: christophe.vallee@cea.fr

by increasing the traditional 13.56 MHz RF frequency. Goto *et al* proposed a mix of low frequency (LF) and high frequency (HF) to have both a high electronic density and highly energetic ions [3]. Following this work, dual-frequency (DF) reactors have been developed as fine etching tools for microelectronic manufacturing. In that case, the CCP is driven by a HF and a LF source attached to either one or two electrodes. One frequency is chosen to be much higher than the other in order to achieve an independent control of ion bombardment and electron density (i.e. ion flux). More details can be found in the review of Bi *et al* concerning DF capacitive discharges [4].

Many groups have created models and simulated the effect of LF addition on plasma density. Depending on the model assumptions and on the pressure, it was reported that the plasma density may be reduced due to sheath width variation, and that it may also be increased due to highly energetic secondary electrons [5–14]. Booth *et al* showed that if plasma negative ion density is included in the simulation then it can strongly modify the effect of adding LF to HF. They found that a mixture of 27 and 2 MHz RF powers have significant effects on plasma density in an Ar/O_2 mixture, whereas the 2 MHz power weakly increases the electron density when the 27 MHz power is low in an $Ar/C_4F_8/O_2$ plasma [12]. Donkó *et al* also showed how the γ coefficient of the secondary electrons may be used to interpret published papers with contradictory results [13], and they concluded that there is only a small pressure process window for which the effect of secondary electrons on the ionization compensates the frequency coupling effect.

Compared to etching tools, only few papers report the effect of LF addition to an HF source for high-pressure plasma used in deposition processes. The effect of frequency has mainly been studied for the deposition of silicon-based materials such as SiO_2, SiO_xN_y, Si_3N_4 and SiC, with the idea of controlling the stress by modifying the ion bombardment of chemical bonds in the film [14–16]. Most of the reported experiments are not really DF processes since they are using a very high frequency source for the plasma generation with additional RF bias at the substrate holder [17]. As an example, in case of silicon oxynitride deposition, it was reported that thin films deposited with an RF/microwave DF source have a higher surface potential and improved charge retention in comparison to films obtained in an RF mode [18]. Bieder *et al* also studied the MW/RF dual excitation for SiO_2 deposition [19] while Yang *et al* used this dual mode for diamond-like deposition [20]. In their case, this mode was mainly used to control the energies of hydrogen ions and the induced stress in the film, not to improve the dissociation rate of the precursor. Recently, Jin *et al* have studied the effect of DF plasma on SiO_x deposition by adding an ultra-high frequency (320 MHz) source to a 13.56 MHz source [21].

The impact of RF frequency on precursor deposition and PECVD process optimization was discussed in depth by Moisan *et al*, who compared the MW PECVD to the RFPECVD and the parameters determining the optimum frequency of operation [22]. Bieder *et al* have also compared two RF frequencies for SiO_2 deposition [19]. In both case no LF was used and the RF frequency (ω) was always higher than the ion plasma frequency (ω_{pi}) of the precursor and/or ions from the precursor decomposition. Since the excitation frequency has profound effects on the spatial distribution of species and their concentrations, the dissociation of the precursor can strongly be increased by crossing the discharge excitation frequency to the basic ion plasma frequency, ω_{pi}, as suggested by Flamm [1]. Manolache *et al* investigated the chlorine contents of 40 kHz and 13.56 MHz silicon tetrachloride and dichlorosilane plasmas in the 100–500 mTorr range by optical emission spectroscopy (OES) [23]. They found the concentration of free chlorine in the dichlorosilane plasma to be much higher at the low RF range and drew conclusions about potential routes that can be developed for frequency-controlled molecular fragmentation. This route is considered here, with comparison and discussion of the improvements brought by DF LF/RF plasma in TiN deposition thanks to the modification of the precursor's decomposition reaction. For this study, we used the 300 mm industrial PECVD tool from Altatech Semiconductor. This is a capacitive plasma chamber with a DF source: 13.56 MHz and 350 kHz. The LF was chosen in order to be lower than the ion plasma frequency of the precursor. The impact of LF addition on plasma density and precursor dissociation are discussed thanks to OES monitoring of the plasma during the process.

2. Experiments

Sample depositions were made with the AltaCVD Advanced Materials™, 300 mm pulsed PEMOCVD chamber presented figure 1, from Altatech Semiconductor. This deposition module consists of two main parts: an evaporating furnace and a deposition chamber. The evaporating furnace is used to change the phase of the precursor from liquid to gas, by decompression and heating, before the introduction of the precursor to the deposition chamber. The liquid precursor is carried by a He gas vector to the evaporating furnace. The mixture then enters the deposition chamber through the shower head. Reactant gases are brought into the deposition chamber through a second level in the shower head, so that it mixes with the precursor only when above the substrate. The pressure in the chamber is kept constant at 2 Torr, resulting in a narrow sheath, far from the substrate. Two independently controlled generators are used with frequencies of 13.56 MHz and 350 kHz, for RF and LF plasma, respectively. Both generators deliver the power at the shower head, the substrate heater being grounded. For discussion of the experimental results, the plasma power given here corresponds to the input plasma power minus the reflected power.

PEMOCVD allows the deposition of carbo-nitride alloys of metals [24], with a variation of the composition depending on the plasma power. In the PEMOCVD process, first the chamber is filled with Ar and He inert carrier and H_2 reactant gases, before plasma activation. Then precursors in a vapour phase are introduced to the chamber and have to go through the plasma to reach the substrate. Plasma energy allows an activation of the first reactions leading to the decomposition of the molecules; second reactions are taking place at the substrate surface, i.e. at 350 °C. The precursor used in this study is a titanium metal–organic precursor, thus the titanium atom in the

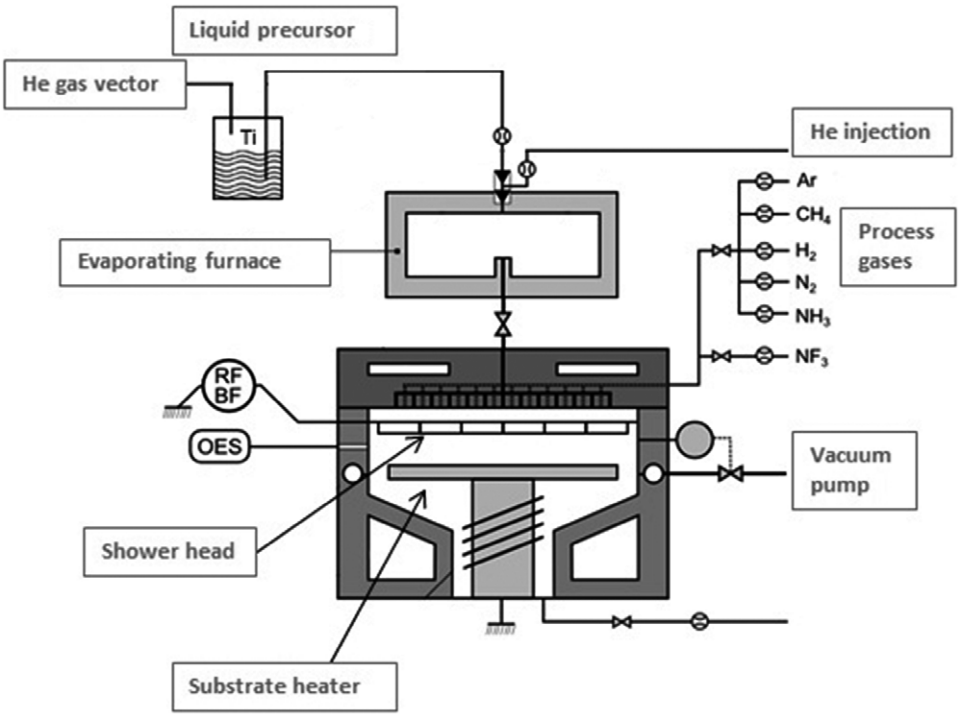

Figure 1. Schematic representation of the 300 mm AltaCVD 300 chamber.

precursor molecule is only bonded with nitrogen atoms; there are no direct bonds with the ethane groups. All depositions were made on 300 mm silicon (1,0,0) prime wafers.

Plasma emission was monitored by OES, with a signal acquisition from 200 to 800 nm at a frequency of one spectrum per second, and gives an insight into the plasma chemistry.

The thickness, density and roughness of deposited films were obtained by careful fitting between theoretical model curves and x-ray reflection (XRR) experimental spectra; resistivity was measured with a four point probe; chemical composition and chemical bonding were analysed by x-ray photoelectron spectroscopy (XPS).

XPS acquisition was done with a quasi-*in situ* tool, which limits TiN oxidation and carbon contamination introduced at the vacuum break [25], thus no oxygen or carbon removal was performed before analysis. Carbon C1s, situated at 285 eV, was used to remove any possible binding energy shift from the charging sample. Bonding environments of Ti, C, N and O were analysed using the Ti2p, C1s, N1s and O1s core-level energy regions, respectively. XPS deconvolution was done using the following constraints for Ti2p: $Ti2p^{5/2}$ and $Ti2p^{3/2}$ are separated by a shift in bonding energy of $\Delta E = 5.54$ eV and an area ratio of 0.5.

3. Plasma modification

In order to discuss the plasma modification induced by LF power and added to the RF power, three plasmas were analysed: pure argon plasma, Ar + H_2 plasma and Ar + H_2 + precursor plasma. Hydrogen in the plasma deposition was used for the removal and control of the carbon content in the TiN films. All the plasmas' emission intensities were recorded by OES as a function of RF power (from 0 to 500 W) and as a function of LF power (from 0 to 100 W) added to 200 W RF power.

3.1. Impact of LF addition on pure Ar plasma

As introduced before, LF addition to RF can enhance the precursor decomposition in the plasma thanks to the modification of the electronic density or electronic temperature. The LF field can also penetrate into the plasma volume resulting in an increased heating of heavy ions (from precursor dissociation). We therefore first monitored the influence of LF addition on pure Ar plasma in order to discuss the role of LF addition on electron density or temperature modification. The 200–800 nm optical emission spectra were recorded as a function of RF and RF + LF powers. The evolutions of two emitted peaks are mainly discussed here: the Ar* emission line at 419.8 nm, which corresponds to the transition from $Ar(3p_5)$ to $Ar(1s_4)$, and the Ar^{+*} emission line at 434.8 nm. The Ar* line has already been found to be a good probe to determine the plasma density in CCP sources as a function of driving frequency [26].

For pure Argon plasma, we can write that the optical emission of Ar originates from the direct electron impact excitation of the Ar atom, and the emission process of Ar* $[3p^5 5p(3p_5) \rightarrow 3P^5 4s(1s_4)]$ by the electron impact is [27]

$$\mathrm{e} + \mathrm{Ar}\left[3\mathrm{p}^6\left({}^1\mathrm{S}_0\right)\right] \xrightarrow{E>14.57\mathrm{eV}} \mathrm{Ar}\left[3\mathrm{p}^5 5\mathrm{p}\left({}^3\mathrm{p}_5\right)\right] + \mathrm{e}$$

$$\downarrow$$

$$\mathrm{Ar}\left[3\mathrm{p}^5 4\mathrm{s}\left({}^1\mathrm{s}_4\right)\right] + h\nu\,(419.8\,\mathrm{nm})\,.$$

Therefore the light emission intensity is proportional to the density of Ar species in the electronically excited

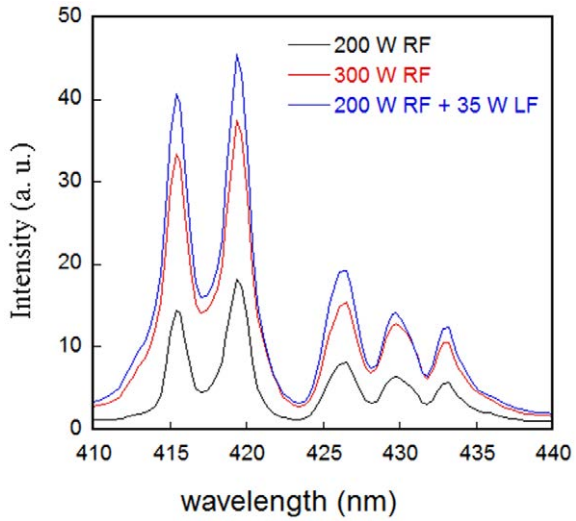

Figure 2. OES of the AltaCVD Ar plasma in the 410–440 nm spectral range.

state: $I_{Ar*}(419\,\text{nm}) = k[Ar^*]$ and the density of excited states $[Ar^*]$ is proportional to the density of Ar ground state species times the efficiency of the plasma η_F: $[Ar^*] = \eta_F[Ar]$. Finally, we have: $I_{Ar*}(419\,\text{nm}) = k\eta_F[Ar]$. The efficiency of the plasma to excite species depends on the electron density and energy distribution (temperature, T_e). In our experimental conditions, for pure Ar plasma as a function of plasma RF power, if electron temperature variation is neglected, then the Ar^* intensity can be directly correlated to the electron density. When LF is added to RF, the electron temperature can be modified due to different mechanisms for sustaining the discharge (secondary electrons versus an electron reflected by an oscillating sheath, see the discussion hereafter). Unfortunately, at the moment it is not possible to measure the effect of LF addition on T_e, so that the Ar^* intensity variations will be correlated here to electronic density variations.

The impact of RF and LF power on Ar spectra is illustrated in figure 2, from 410 to 440 nm. In this figure, one can compare the evolution of the intensity of the OES bands when going from 200 W RF to 300 W RF and from 200 W RF to 200 WRF + 35 WLF. In both cases, an increase in the intensity was observed when increasing the power injected into the plasma. But it appears that higher intensities were obtained with LF added to RF. A simple explanation is that higher plasma densities are obtained with LF addition instead of RF addition to the 200 W RF power. In this case, we made the assumption that electron temperature is not modified when adding LF. This should be verified in the future.

Figure 3(*a*) shows the evolution of the Ar^* (419.8 nm) emission line as a function of RF power and RF (200 W) + LF power. Figure 3(*b*) shows the evolution of Ar^{+*} (434.8 nm). In figure 3(*a*), with RF power only, the relation between plasma power and plasma intensity is of a square root type. Before 30 W, there is not enough energy to switch on the plasma; above 50 W one can see a quite linear relation. Such a relation between plasma power and intensity is characteristic of CCP reactors. Godyak and Piejak have shown that a CCP discharge is dominated by Ohmic heating at high pressure (versus stochastic at low pressure) [28]. In this case, the plasma density, n_0, can be correlated to the RF frequency, ω, and the applied RF voltage, V_0, by the following equation (see [29] for more details on RF plasma):

$$n_0 \propto \omega^2 V_0^{\frac{1}{2}} \tag{1}$$

The same evolution is observed for the Ar^{+*} emission line as a function of RF power in figure 3(*b*).When LF power was added to 200 W RF power, strong modifications were observed. As an example, the ratio I(419.8 nm–300 W RF)/I(419.8 nm–200 W RF) is equal to 1.37, while the ratio I(419.8 nm–200 W RF + 100 W LF)/I(419.8 nm–200 W RF) is equal to 2.17. The same evolution is obtained with the Ar^{+*} emission, going from a value of 1.48 to 2.27.

As said in the introduction, some authors have reported that the addition of LF to RF power may increase the plasma density due to highly energetic secondary electrons. Thus the discharge is not dominated by Ohmic heating. The transition in the CCPRF source toward a regime dominated by secondary electrons (also called the 'γ-regime') has been studied in the past [30–34]. As an example, Belenguer and Boeuf studied the case of helium (3 Torr) plasma, and they clearly showed that two different regimes may exist [35]. The transition from one regime to the other depends on the energy obtained by the electrons in the sheath and their ability to ionize. It means that a large sheath (thus high power) and high pressure help to shift the plasma in the direction of the γ-regime. Godyak *et al* were able in their plasma to have a γ-regime transition when increasing the voltage to values higher than 400 V in a pure helium plasma at 3 Torr [36]. Belenguer and Boeuf were able to fit the experimental curves when the effects of secondary electrons were taken into consideration, with an emission coefficient, γ, of 0.08 [35].

In our experiments, the high-pressure regime may have helped to obtain the γ-regime. Moreover, LF addition may have increased the sheath width, which is also in favour of the γ-regime. In order to confirm that Ar^* intensity enhancement can be linked to the transition to a γ-regime when LF is added, OES measurements were performed at higher RF power. As seen in figure 4, for RF power higher than 400 W, a modification of the Ar^* intensity variation was observed, with again a fast increase of the Ar^* intensity. This can be interpreted as a transition to a γ-regime in single RF plasma when the power is higher than 400 W. A power of 400 W seems to be the threshold above which the discharge is sustained by secondary electrons. At these higher RF powers, the Ar^* intensity now follows the same law as the one obtained with LF addition. Therefore, in our experimental conditions, the plasma density increases by LF addition thanks to secondary electrons. This behaviour is contrary to what was obtained by numerical models at low pressure (see [7] for example). However, this result is in good agreement with recent papers from Ahn and Chang [37], Xiang-Mei *et al* [38] and Schulze *et al* [31].

3.2. Impact of LF addition on Ar + H_2 plasma

Contrary to pure Ar plasma, when adding LF to RF in an Ar + H_2 plasma, the intensity of the Ar^* emission lines

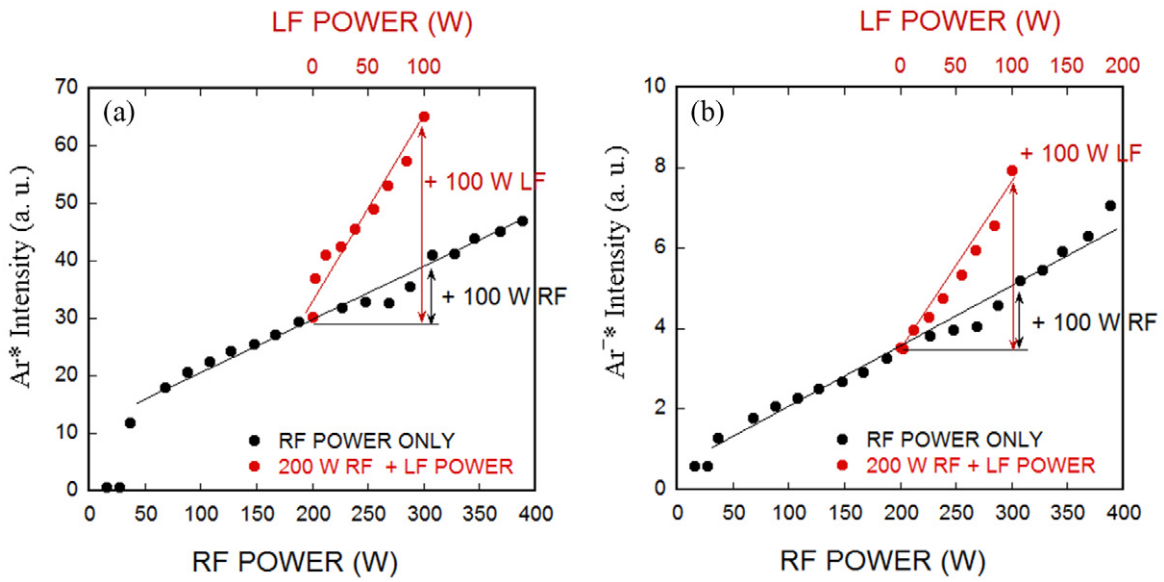

Figure 3. Evolution of the Ar* (*a*) and Ar^{+*} (*b*) emission lines as a function of RF power and 200 W RF + LF power.

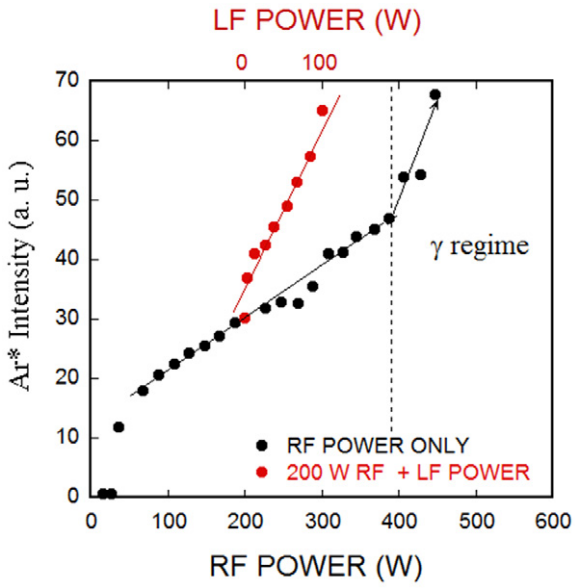

Figure 4. Evidence of a γ-mode transition for a pure Ar plasma at 400 W with single RF power and at 200 W with dual RF and LF power.

decreased with LF addition (easily observed for the 750 nm Ar* emission line; see figure 5(*d*) for example). This may indicate a decrease of electron density or electron temperature with LF addition, which is contradictory with what was observed in pure Ar plasma; this point will be discussed later (see equations (2)–(5)). The H_2 continuum from the primary system in the 300–500 nm range (see figure 6) also decreased with LF power. New emission peaks were also observed with LF power addition—some are highlighted by an arrow in figures 5(*a*) and (*b*). In the 400–500 nm range, the new peaks observed can be attributed to the H_2 secondary system ($G^1\sum_g^+ - B^1\sum_u^+$) [39]. The H_α emission peak from Balmer lines at 656.3 nm also increased with LF power indicating an increase of H atomic species in the plasma. This increase can be correlated to the intensity decrease of the Ar* emission line and may finally be the consequence of the high level of excited argon activating the dissociation of H_2 in our experimental conditions. We can therefore explain the opposite behaviour of Ar* at 750 nm and H* by the H_2 dissociation from collisions with Ar* following the reaction proposed by [40]:

$$Ar(^2P_1) + H_2 \rightarrow Ar(^1S_0) + 2H. \quad (2)$$

And in a more general way, we can write for Ar* excited species and Ar_m metastable species the reaction rate that may occur in the Ar/H_2 plasma [41–43]:

$$Ar^* + H_2 \rightarrow Ar + 2H \quad (3)$$

$$Ar_m + H_2 \rightarrow Ar + 2H. \quad (4)$$

This increase of H density in the plasma may be of importance for the PECVD process since H atoms might break different bonds in the precursor molecule than in pure RF plasma conditions.

3.3. Modification of optical emission spectra for Ar + H_2 + Ti precursor

Figure 7 shows the modification in the OES when adding a Ti precursor in the gas phase. Figure 7(*a*) is a comparison between 200 W RF plasmas with and without a precursor. The OES spectrum in the 300–500 nm range shows that a new emission peak could now be observed at 386 nm (indicated by an arrow in figure 7(*a*)). This peak corresponds to the CN* emission band from the violet band system [39].This is not surprising since CN bonds are present in the Ti precursor. No Ti* emission line is observed at 363.5 nm, indicating that the precursor is probably not completely dissociated in the plasma phase, this result being in contradiction with what was reported by Rie *et al* [44]. The intensity of H* atomic species was

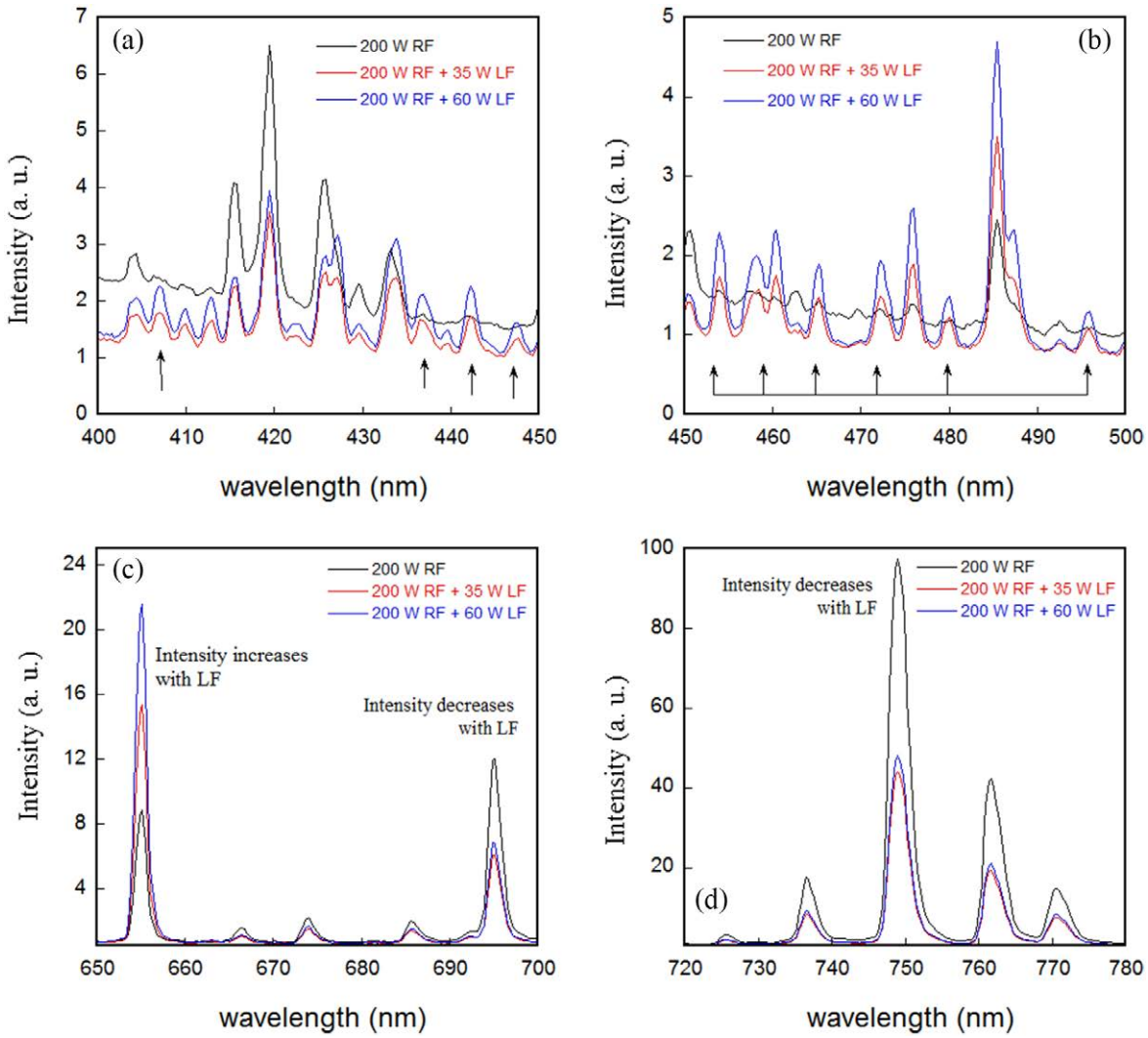

Figure 5. The impact of LF addition in Ar + H_2OES in four spectral ranges: (*a*) 400–450 nm; (*b*) 450–500 nm; (*c*) 650–700 nm; and (*d*) 720–780 nm. Arrows in the figures indicate new emission peaks.

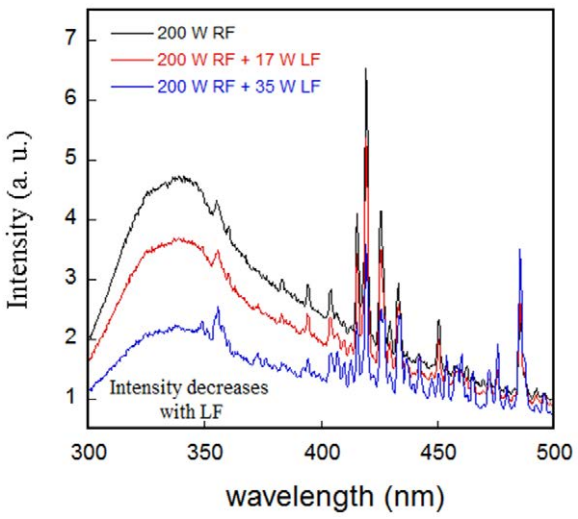

Figure 6. The impact of LF addition in Ar + H_2OES in the 300–500 nm range.

observed to decrease when adding Ti in the gas phase. This can be seen in figure 7(*a*) with the decrease of H_β emission line from the Balmer lines at 486.1 nm and the H_α line at 656.3 nm (figure 8(*d*)). It is not surprising since we expect that the H atoms react with carbon-based radicals from the precursor in order to limit the C, H and reaction by-product content in the growing film.

The same spectral range for a 200 W RF + 60 W LF plasma, with and without a Ti precursor added to the Ar + H_2 plasma, is presented in figure 7(*b*). A new CN^* emission band clearly appears at 386 nm. Another new weak emission peak is observed at 336 nm and can be attributed to a weak emission from the NH^* band [39], indicating that the precursor dissociation is modified when adding LF to RF. The comparison in all the spectral ranges shows new weak peaks at 402 nm, 446 nm (see the arrows in figure 8(*a*)), 491 nm and 586 nm. These peaks are due to He^* emission, such as He ($3d^3D \rightarrow 2p^3P_0$) at 587.6 nm. Helium was used in the process as a gas carrier for the liquid injection of the Ti precursor. As of today, no explanation for the presence of emitted He^* in the DF mode and not the RF mode has been found. However,

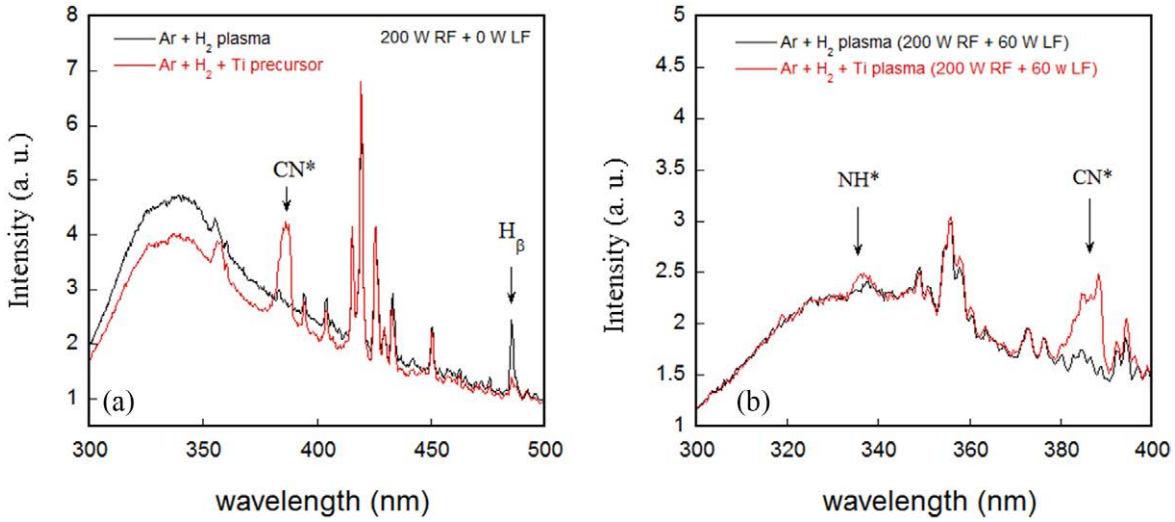

Figure 7. (*a*) A comparison for a 200 W RF plasma with and without a Ti precursor. (*b*) The impact of the Ti precursor for a 200 W RF + 60 W LF plasma.

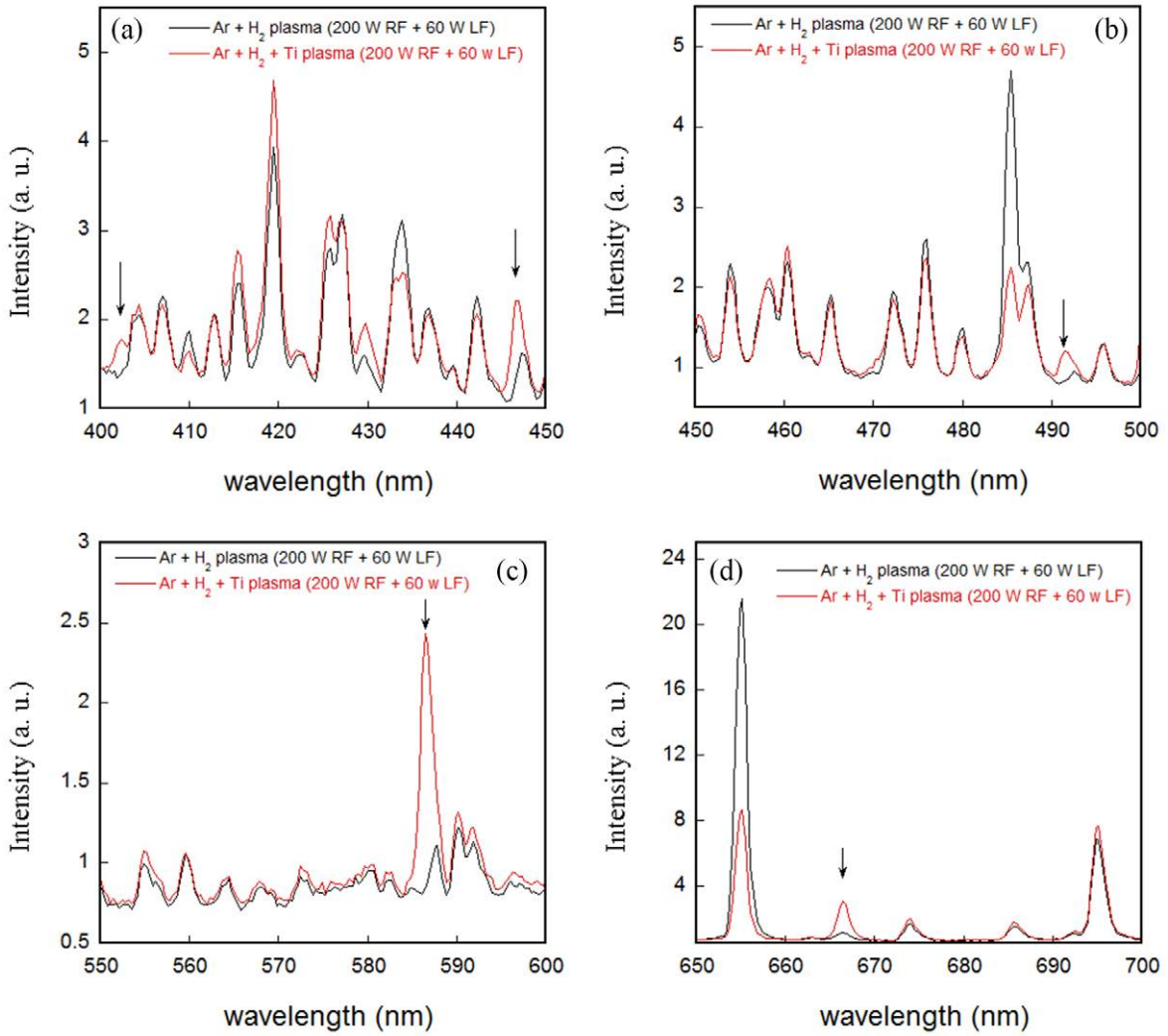

Figure 8. Effect of Ti precursor addition in the OES of the 200 W RF + 60 W LF plasma: (*a*) the 400–450 nm range; (*b*) the 450–500 nm range; (*c*) the 550–600 nm range; (*d*) the 650–700 nm range.

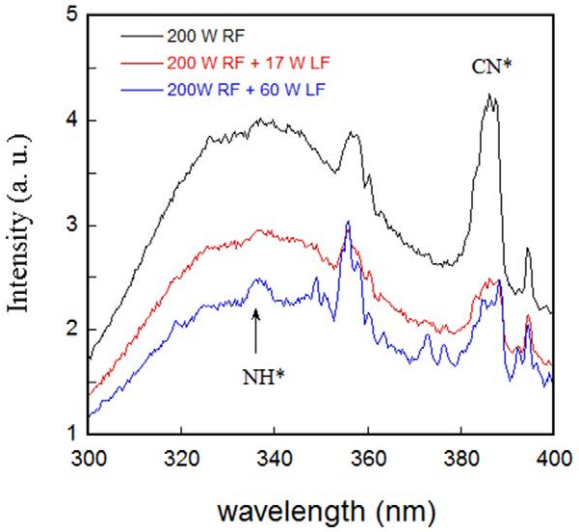

Figure 9. Evolution of the OES of Ar + H_2+Ti precursor plasma with LF power.

Table 1. Evolution of thickness, density and resistivity with increase of RF plasma power.

RF power (W)	Deposition rate (Å s^{-1})	Density (g cm^{-3})	Roughness (Å)	Resistivity (mΩ cm)
200	1.03	3.38	26.2	110
250	1.25	3.34	27.1	93
300	1.60	3.35	27.4	64

as for pure argon plasma, it shows that the plasma is strongly modified by LF addition.

Figure 9 shows the evolution of OES spectra in the 300–400 nm range as a function of LF power added to RF power. Some of the new peaks are correlated to new emission from the H_2 plasma as previously observed, and the only two new peaks which came into view with the introduction of the precursor are NH* at 336 nm and CN* at 386 nm.

In summary, we showed that LF addition to RF power increases the Ar plasma density. This can be interpreted by a transition to the γ-mode due to secondary electrons' heating. In the Ar/H_2 plasma, the LF addition helped to increase the H density in the plasma by a H_2 dissociative collision with excited Ar or metastable Ar. Finally, the TiN precursor was not completely dissociated in our discharge and in the dual mode, but new excited species were observed, indicating a different fragmentation of the precursor. We will now examine the effect of the LF addition on the TiN film properties.

4. Thin TiN film analysis

As for the OES analysis, we first discuss the properties of thin TiN films deposited in the pure RF mode. Then, properties of TiN films obtained in the dual mode will be analysed and compared to the RF ones.

4.1. Impact of RF power on film properties

Table 1 gives the deposition rate, density, roughness and resistivity of TiN layers obtained for RF plasma power between 200 and 300 W.

As usually observed in PECVD, increasing the RF power improves the dissociation of the precursor and increases the deposition rate [44]. The growth rate increased by a factor of 1.55 from 200 to 300 W, quite similar to the plasma density evolution (Ar* line, section 3.1) of 1.37. In parallel to the growth rate evolution, the resistivity decreased when the RF power increased: its value was reduced from 110 to 64 mΩ cm. Roughness of the thin TiN films is only slightly modified by RF power, with little variation (from 26.2 to 27.4 Å). Finally, increasing the plasma power does not affect density, which is low compared to the theoretical density of TiN: 5.40 g cm^{-3} [45]. A high level of oxidation has to be taken into account for density calculations, as it reduces the density (TiO_2: 4.23 g cm^{-3} [45]) and can partly explain the low density measured. Moreover, theoretical densities are calculated for a perfectly crystalline material, whereas the obtained TiN is amorphous (confirmed by x-ray diffraction, not shown here) with a lower density.

Hence, a possible hypothesis to explain the improvements observed is that the increase in plasma power may improve the by-products' removal during deposition leading to the easier nucleation of the layer and to a reduction of resistivity. Indeed, the presence of carbon from reaction by-products in the layer decreases the conductivity of the layer.

The XPS analysis of TiNRF 200, 250 and 300 W layers is discussed in section 4.3.

4.2. Impact of LF power addition to RF plasma on thin film properties

To evaluate the impact of LF addition to RF plasma on TiN material deposition and to be able to compare it with the increase in RF plasma power, all deposition parameters were unchanged, and only LF power was added to 200 W of RF power. Figure 10 shows the deposition rate obtained with and without LF addition. Figure 11 shows the impact of the DF mode on resistivity while figure 12 illustrates the beneficial role of LF addition on thin films' density. The fitting error from XRR spectra is at maximum 10%, thus is not significant and is not reported in figures 10 and 12. The error bars in figure 11 correspond to the resistivity uniformity measured with 1 cm edge exclusion.

It is clear from figures 10–12 that strong modifications are obtained with LF addition. Again we can correlate the higher deposition rate in the DF mode to the higher electron density of the plasma. In the single RF mode with the addition of 100 W RF (from 200 to 300 W), the deposition rate increases by 60%, but with only 60 W LF added, the deposition rate is increased by 126%. And whereas an increase of RF power from 200 to 300 W leads to an increase in the deposition rate only, adding LF power to the plasma allows us to increase both the deposition rate and the density of the layer, as shown in figure 12. An increase of both deposition rate and density indicates that the reaction mechanism is more efficient,

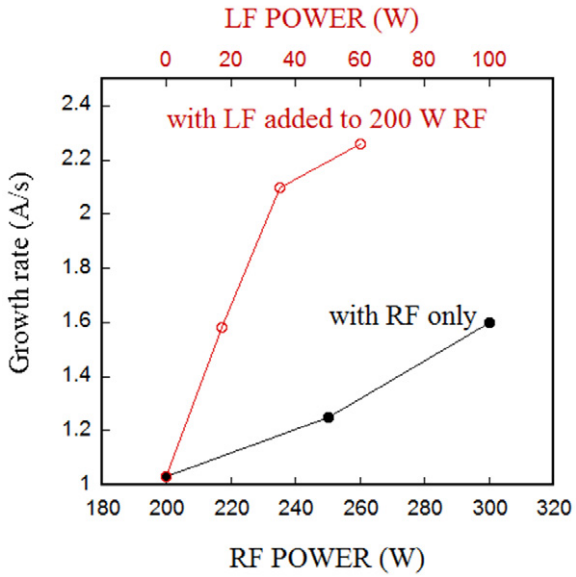

Figure 10. TiN deposition rate in RF mode and DF mode with LF addition.

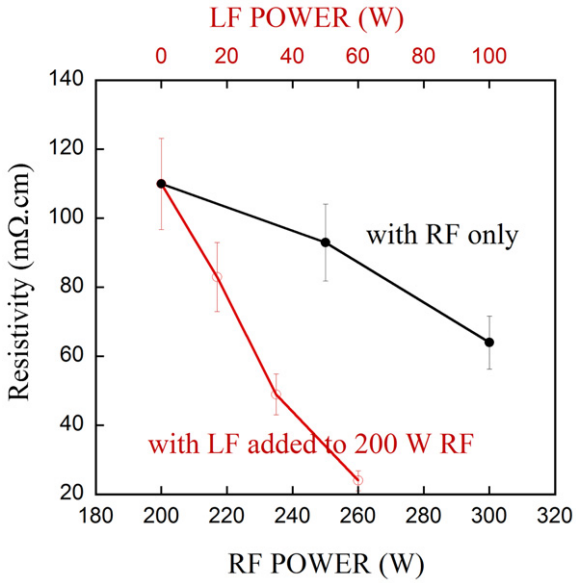

Figure 11. TiN resistivity in RF mode and DF mode with LF addition.

i.e. more material is deposited on the substrate. However, above 35 W of added LF plasma power, the deposition rate and density do not have a linear growth with the plasma power increase. There is a change in the slope for all the characteristics of the material after 35 W of added LF, toward a lower augmentation of the deposition rate and resistivity but a higher density.

The addition of LF plasma also has an important effect on sheet resistivity. Indeed, an increase in RF plasma power from 200 to 300 W reduces the resistivity by a factor of two. Such a reduction is obtained with only 35 W of LF plasma power, and adding 60 W of LF plasma power reduces the resistivity by a factor of five. This decrease in resistivity is partly linked to the density of the layer; a material has its optimum conductivity when it is the closest to the theoretical density.

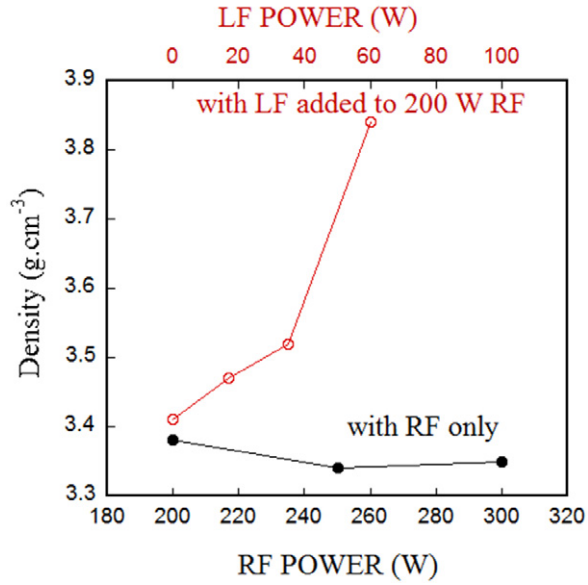

Figure 12. TiN density in RF mode and DF mode with LF addition.

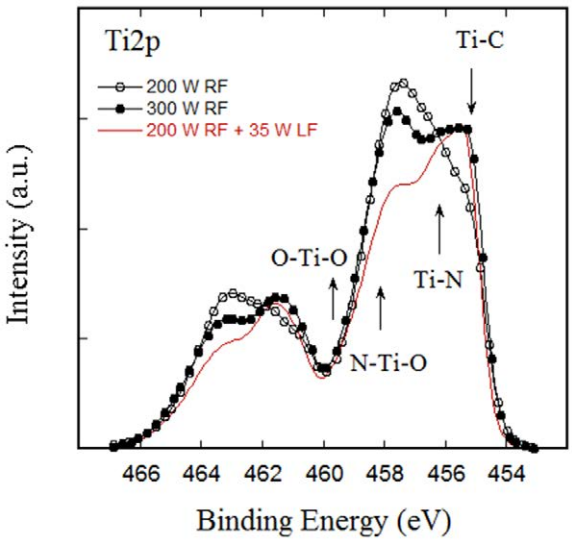

Figure 13. XPS Ti2p spectra of TiN samples.

4.3. Impact of LF power addition to the RF plasma reaction mechanism

The impact of LF on chemical composition was studied by XPS on TiN materials. Figure 13 presents the Ti2p spectra of samples deposited with 200 W RF, 300 W RF and 200 W RF + 35 W LF.

Bonding environments corresponding to each peak are noted in figure 13. TiO_2, TiON, TiN and TiC are located at 459.6 eV, 458 eV, 456 eV and 454.9 eV, respectively [46].

In figure 13, it appears that an RF power increase from 200 to 300 W favours the creation of TiN, resulting in lower TiON formation. Then, LF plasma power addition to 200 W RF also reveals important changes. First the Ti–N bonds increase and the TiON bonds are reduced. If the LF sample is compared to a sample with 300 W RF power, it appears that the TiN creation is similar; however, an additional 100 W of RF are used,

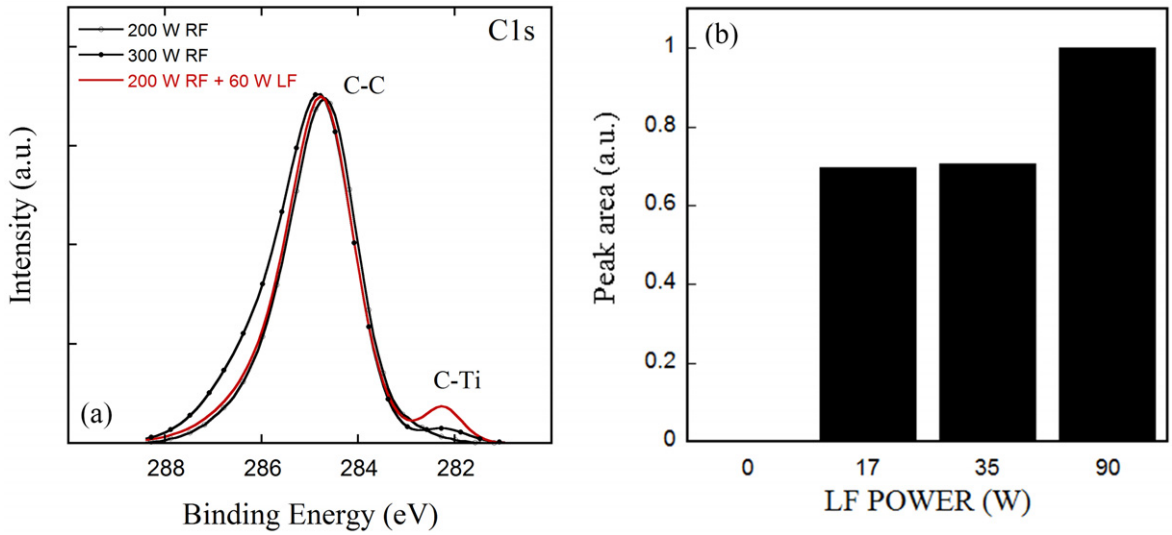

Figure 14. C1sXPS spectra (*a*) and evolution of the area of the Ti–C bonding environment (*b*).

compared with the 35 W of LF. The second important change is the shift of the TiN peak maximum towards lower energies, when RF is increased or LF plasma is added. This shift may correspond to the creation of the TiC bonding environment. However, due to the low number of bonds created, the new environment TiC is not observed as a new peak.

XPS measurements were also performed a second time, after a several hours' vacuum break, to compare the oxidation uptake of each sample. The spectra are not presented here, as no significant difference between the samples was observed. Thus, oxygen uptake is similar no matter which plasma was used for deposition.

The Ti2p modifications previously observed are compared with the evolution of the C1s XPS spectrum with LF power increase, presented in figure 14(*a*). Evolution of the C–Ti peak area, which corresponds to the number of carbon atoms bonded with titanium, is given in figure 14(*b*).

The C1s spectra in figure 14(*a*) clearly highlight the formation of TiC bonding when using LF plasma, with a C–Ti environment at 282 eV [46]. The intensity of the Ti–C peak confirms the supposition of low TiC content in the layer and the impossibility of observing the TiC peak in the Ti2p spectrum. Moreover, an increase of the LF plasma power leads to a higher TiC peak, as seen on the evolution of the peak area of C bonded with Ti, shown in figure 14(*b*). Changes on N1s spectra, not shown here, are not as visible; only a shift towards lower energy of N–Ti bonding is apparent. This shift corresponds to the increase of TiN bonds and the decrease of TiO environments, as seen on the Ti2p spectra in figure 13.

Two explanations can support the presence of new TiC bonds in the materials. First, this can be due to the modification of the Ti precursor dissociation in the plasma phase (as observed by OES with new emission peaks) and so modifications of elastic and inelastic collisions in the plasma phase thanks to electronic density and temperature modifications with LF addition. Moreover, the ion plasma frequency (f_{pi}) of the precursor, and heavy ions coming from the precursor dissociation, is a few MHz. Thus the LF

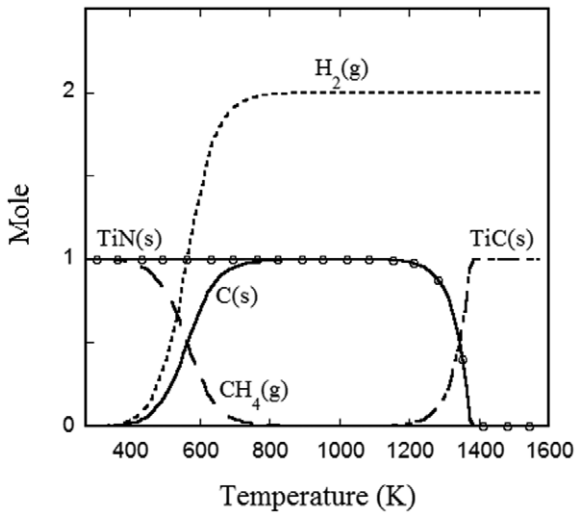

Figure 15. Evolution of the Gibbs energy of the products from equation (5).

field can penetrate into the plasma volume causing increased heating of heavy ions and increased dissociation. This is in agreement with papers from Flamm [1] and Manolache *et al* [23]. The second mechanism can entail heterogeneous reactions, i.e. reactions at the surface of the growing film. Hence, the TiC formation can be due to the activation of a transposition mechanism, from the metal–organic titanium precursor, following equation (5) [47]:

$$\mathrm{TiN} + \mathrm{CH_4\,(g)} \rightarrow \mathrm{TiC} + 1/2\mathrm{N_2\,(g)} + 2\mathrm{H_2\,(g)}\,. \qquad (5)$$

Since the deposition is done at 350 °C and at 2 Torr, it is possible to determine the Gibbs energy of reaction (5) to be +75 kJ mol^{-1}. This reaction is not spontaneous, but TiC formation is favoured at higher temperatures, as shown in figure 15. The calculations indicate that the transposition reaction (5) threshold is 970 °C. Such a high temperature is not supposed to be reached at the surface of the sample, even

when the energy brought by the hydrogen plasma is taken into consideration.

Consequently, the hypothesis of surface heating by plasma leading to a transposition reaction is not realistic. The creation of TiC bonds in the plasma phase has to be preferred.

Also, an increase of RF plasma power from 200 to 300 W does not show any creation of TiC bonds, whereas an addition of 17 W of LF plasma power to 200 W RF is sufficient to create TiC bonds, as shown in figure 14(a). As a consequence, a hypothesis of higher efficiency of the decomposition of the precursor's molecules in a DF mode, with a LF source lower than the f_{pi} of the precursor, can be made.

This reduction of the plasma power needed to create material with lower resistivity is welcome for some of the applications, i.e. plasma was proven to be the source of damage on the dielectric, resulting in poor electrical characteristics when used for CMOS technologies [48].

5. Conclusion

In the case of a PECVD process, we have shown that using a dual-frequency mode instead of a single RF mode is a very good method of enhancing the deposition rate and film properties, such as density and resistivity. It has been shown that modification of the properties of a TiN metal are obvious with the DF mode: the film is deposited faster and it has a higher density and lower resistivity. In the case of pure argon plasma, the optical emission spectroscopy of the plasmas has shown that the DF mode increases the plasma density. This is explained by a transition to a γ-mode in the CCPD discharge thanks to secondary electrons. The H atoms' density is also higher in the DF mode. Finally, new emitted peaks are observed. These can be correlated to a modification of the Ti precursor dissociation in the DF mode. As a consequence, new bonds are also observed in the growing film. To conclude, and as suggested in 1986 by Flamm [1] and shown by Manolache *et al* [23], the dissociation of a precursor may be strongly increased by adding a discharge excitation frequency, ω_{pi}, of the ionized precursor to the basic ion plasma frequency.

References

[1] Flamm D L 1986 *J. Vac. Sci. Technol.* A **4** 729
[2] Surendra M and Graves D B 1991 *Appl. Phys. Lett.* **59** 2091
[3] Goto H H, Lowe H D and Ohmi T 1992 *J. Vac. Sci. Technol.* A **10** 3048
[4] Bi Z-H, Liu Y-X, Jiang W, Xu X and Wang Y-N 2011 *Curr. Appl. Phys.* **11** 52
[5] Georgieva V and Bogaerts A 2005 *J. Appl. Phys.* **98** 023308
[6] Lee J K *et al* 2004 *IEEE Trans. Plasma Sci.* **32** 47
[7] Boyle P C, Ellingboe A R and Turner M M 2004 *J. Phys. D: Appl. Phys.* **37** 697
[8] Kim H C, Lee J K and Shon J W 2003 *Phys. Plasmas* **10** 4545
[9] Turner M M and Chabert P 2006 *Phys. Rev. Lett.* **96** 205001
[10] Robiche J *et al* 2003 *J. Phys. D: Appl. Phys.* **36** 1810
[11] Kawamura E, Lieberman M A and Lichtenberg A 2006 *Phys. Plasmas* **13** 063510
[12] Booth J P, Curley G, Marié D and Chabert P 2010 *Plasma Sources Sci. Technol.* **19** 015005
[13] Donkó Z, Schulze J, Hartmann P, Korolov I, Czarnetzki U and Schüngel E 2010 *Appl. Phys. Lett.* **97** 081501
[14] Iliescu C, Chen B, Poenar P P and Lee Y Y 2008 *Sensors Actuators* B **129** 404
[15] Tan W S, Houston P A, Hill G, Airey R J and Parbook P J 2004 *J. Electron. Mater.* **33** 400–7
[16] Pearce C W, Retcho R F, Gross M D, Koefer R F and Pudliner R A 1992 *J. Appl. Phys.* **71** 1838–41
[17] Martinu L, Klemberg-Sapieha J E, Küttel O M, Raveh A and Wertheimer M R 1994 *J. Vac. Sci. Technol.* A **12** 1360–4
[18] Kressmann R, Amjadi H, Sessler G M, Rats D, Martinu L, Klemberg-Sapieha J E and Wertheimer M R 1998 *Annual Report Conf. on Electrical Insulation and Dielectric Phenomena (Atlanta, Georgia)* vols1 and 2, pp 605–8
[19] Bieder A, Gruniger A and von Rohr Ph R 2005 *Surf. Coat. Technol.* **200** 928–31
[20] Yang L, Xin Y, Xu H, Yu Y and Ning Z 2010 *Plasma Sci. Technol.* **12** 53–8
[21] Jin S B, Lee J S, Choi Y S, Choi I S and Han J G 2011 *Thin Solid Films* **519** 6334–8
[22] Moisan M, Barbeau C, Claude R, Ferreira C M, Margot J, Paraszczak J, Sa A B, Sauvé G and Wertheimer M R 1991 *J. Vac. Sci. Technol.* B **9** 8–25
[23] Manolache S, Sarfaty M and Denes F 2000 *Plasma Sources Sci. Technol.* **9** 37–44
[24] Kafizas A, Carmalt C J and Parkin I P 2013 *Coord. Chem. Rev.* **257** 2073–119
[25] Pelissier B, Kambara H, Godot E, Veran E, Loup V and Joubert O 2008 *Microelectron. Eng.* **85** 151–5
[26] Kitajima T, Takeo Y, Nakano N and Makabe T 1998 *J. Appl. Phys.* **84** 5928–36
[27] Kakuta S, Makabe T and Tochikubo F 1993 *J. Appl. Phys.* **74** 4907–14
[28] Godyak V A and Piejak R B 1990 *Phys. Rev. Lett.* **65** 996
[29] Chabert P and Braithwaite N 2011 *Physics of Radio-Frequency Plasmas* (Cambridge: Cambridge University Press) ISBN 9780521763004
[30] Boeuf J P and Belenguer Ph 1992 *J. Appl. Phys.* **71** 4751
[31] Schulze J, Donko Z, Luggenhölscher D and Czarnetzki U 2009 *Plasma Sources Sci. Technol.* **18** 034011
[32] St Braithwaite N, Haas F A and Godyear A 1998 *Plasma Sources Sci. Technol.* **7** 471
[33] Surendra M and Graves D B 1991 *IEEE Trans. Plasma. Sci.* **19** 144
[34] Böhm C and Perrin J 1991 *J. Phys. D: Appl. Phys.* **24** 865
[35] Belenguer Ph and Boeuf J P 1990 *Phys. Rev.* A **41** 4447
[36] Godyak V A and Kanneh A S 1986 *IEEE Trans. Plasma Sci.* **PS-14** 112
[37] Ahn S K and Chang H Y 2009 *Appl. Phys. Lett.* **95** 111502
[38] Xiang-Mei L, Yuan-Hong S and You-Nian W 2011 *Chin. Phys.* B **20** 065205
[39] Pearse R W B and Gaydon A G 1976 *The Identification of Molecular Spectra* 4th edn (London: Chapman and Hall)
[40] Schaffnit C, Thomas L, Rossi F, Hugon R and Pauleau Y 1998 *Surf. Coat. Technol.* **98** 1262
[41] Delcroix J L, Matos-Ferreira C and Ricard A 1975 *Atomes et molécules métastables dans les gaz ionisés* (Paris: éditions du CNRS) p 197 chapter 5
[42] Watanabe T and Katsuura K J 1967 *Chem. Phys.* **47** 800
[43] Fink E H, Wallach D and Moore C B 1972 *J. Chem. Phys.* **56** 3608
[44] Rie K T and Wöhle J 1999 *Surf. Coat. Technol.* **112** 226
[45] Material Property Data 2013; available at www.matweb.com
[46] Moulder J F, Stickle W F, Sobol P E and Bomben K D 1992 *Handbook of X-Ray Photoelectron Spectroscopy* (Waltham, MA: Perkin-Elmer Corporation)
[47] Caubet P *et al* 2008 *J. Electrochem. Soc.* **155** 8
[48] Park T J, Kim J H, Jang J H, Na K D, Hwang C S, Kim G M, Choi K J and Jeong J H 2008 *Appl. Phys. Lett.* **92** 202902